Linking formulation feedstock to printability by robocasting: a case study of eco-friendly alumina pastes

Delphine Gourdonnaud, Julie Bourret, Vincent Pateloup, Lisa Giardi, Luc Picton, Vincent Chaleix, Thierry Chartier, Benoit Naït-Ali, Marguerite Bienia, Pierre-Marie Geffroy

Open Ceramics 18 (2024) 100606

Contents lists available at ScienceDirect

Open Ceramics

journal homepage: www.sciencedirect.com/journal/open-ceramics

Linking formulation feedstock to printability by robocasting: A case study of eco-friendly alumina pastes

Delphine Gourdonnaud [a], Julie Bourret [a,*], Vincent Pateloup [a], Lisa Giardi [a], Luc Picton [b], Vincent Chaleix [c], Thierry Chartier [a], Benoit Naït-Ali [a], Marguerite Bienia [a], Pierre-Marie Geffroy [a]

[a] CNRS, Institute of Research for Ceramic (IRCER), UMR 7315, University of Limoges, European Ceramic Center, 12 rue Atlantis, F-87068, Limoges, Cedex, France
[b] University of Rouen Normandie, INSA Rouen Normandie, CNRS, PBS UMR 6270, F-76000 Rouen, France
[c] LABCiS, UR 22722, University of Limoges, 33 rue François Mitterrand, F-87032, Limoges, France

ARTICLE INFO

Handling Editor: Dr P Colombo

Keywords:
Printability
Alumina
Natural polymers
Rheology
Robocasting

ABSTRACT

Robocasting stands as a pertinent additive manufacturing technique for producing intricate ceramic parts. Amidst stricter environmental regulations, the adoption of natural additives becomes imperative. This study investigates the influence of plant-based additives on the rheology and printability of eco-friendly pastes.

Various 50 vol%-alumina pastes were formulated using natural binders, plasticizers and dispersants (*e.g.*, lignosulfonate, polysaccharides, glycerol) and then assessed through oscillation and flow rheological analyses. Paste viscosity and rigidity often deviated from printability maps reported in the literature, showing the complexity of defining universal printability criteria. A comprehensive investigation was conducted on the water retention capabilities of additives, liquid phase migration and paste drying kinetics.

This paper highlights the critical importance of constraining liquid phase migration within eco-friendly ceramic pastes and the crucial role of polymer chain reorientation under shear. Consequently, this research lays diversifying formulations, offering sustainable solutions for industrial ceramic applications.

1. Introduction

Robocasting, also known as the micro-extrusion process, has become a prevalent 3D printing method for producing on-demand parts, with a complex geometry. It enables the implementation of various ceramic materials in diverse fields, including information and communication technologies, healthcare [1,2] or energy [3]. Daily advancements in scientific and technical capabilities continue to expand the possibilities of this technology. For instance, porous structures have been recently printed using zirconia with potato starch and rice starch, thus demonstrating the ability to control the structural organization of pores through tips of 410 μm inner diameter [4]. Wahl et al. [5] have developed pastes with a varying amount of uncoated SiC platelets for the production of reaction-bonded silicon carbide. In both cases, the formulations comprise aqueous systems and typically include conventional additives like Darvan 821A or 670 as dispersants and polyethylene glycol (PEG) as a binder. It is worth noting that the additives used in paste preparation are generally sourced from the petrochemical industry, which can have a negative impact on the environment or the operator's health. As an example, the most commonly used dispersants are polyelectrolytes, such as polyacrylic acid, polyethyleneimine or polymethacrylate [6].

In the industrial sector, legislations governing the use of organic substances are becoming increasingly stringent, whether at the national, European, or global levels, as exemplified by standards such as ISO 14006:2011 or ISO 9001:2008. These regulations often entail substantial additional costs, whether due to the need for upgrading industrial facilities or the introduction of new environmental taxes on waste recycling. In their review paper, Duran et al. [7] highlighted a contemporary approach for addressing the current challenges posed by waste disposal restrictions and stringent environmental regulations. This approach involves the use of substances characterized by low toxicity and a reduction in their amount within ceramic green bodies [7]. Hence, developing materials in alignment with the principles of

Abbreviations: ALS, ammonium lignosulfonate dispersant; P95, psyllium P95; GG, guar gum; DCN, ammonium polymethacrylate dispersant; PL, plastic limit.

* Corresponding author.
E-mail address: julie.bourret@unilim.fr (J. Bourret).

https://doi.org/10.1016/j.oceram.2024.100606
Received 10 January 2024; Received in revised form 9 May 2024; Accepted 10 May 2024
Available online 11 May 2024

green chemistry involves a specific focus on using water-based solvents and environmentally friendly additives. There have been promising research endeavours in this regard that warrant further investigation. Nowadays, traditional petrochemical-derived products can be replaced with plant-based alternatives, as demonstrated by the use of polylactic acid (PLA) for certain bottle applications [8] or the substitution of glass wool with hemp wool. Moreover, despite the frequent use of binders like phenolic resin [9] and polyvinyl butyral (PVB) [10], more eco-responsible formulations, based on cellulose derivatives like ethyl-hydroxyethyl cellulose or methylcellulose, have been extensively reported in the literature [11]. Nonetheless, it is noteworthy that cellulose derivatives themselves are produced through chemical transformations of cellulose.

To move further and advance towards a more sustainable industry, it becomes compelling to substitute all petrochemical-derived additives (*e.g.* dispersant, binder, plasticizer) with more natural components. Plant-based additives are firmly established in the food industry and have already undergone testing in the field of extrusion, such as xanthan [12], psyllium [13] or guar gum [14]. Water-soluble polysaccharides like these are capable of forming a gel-like network, making them well-suited for suspending and binding ceramic particles. As reported in the literature, polymer chains can undergo disentanglement when subjected to sufficient force, thereby influencing the shear-thinning behaviour of the pastes during the robocasting process [15].

However, based on the current state of knowledge, achieving a fully eco-friendly system that includes natural binders, dispersants, plasticizers, etc., remains an ongoing challenge. Furthermore, the complex interactions among polymer chains have not undergone exhaustive investigation and reached complete comprehension [16]. Better understanding these interactions holds the potential to facilitate the development of stable, highly loaded pseudo-plastic ceramic pastes using plant-based additives. Consequently, this could lead to a reduction in the required amount of additives, without compromising the structural and mechanical integrity of the printed parts.

Various studies present the rheological properties of ceramic pastes or suspensions (for example based on alumina) used for micro-extrusion [17–20]. There is a wide variety of rheological methodologies to characterize a paste; one of the most encountered in the literature is the amplitude sweep test. The latter provides access to the viscoelastic properties of a paste, such as the storage modulus (G') or the yield point (τ_y). Hence, some work reported this method as a way to provide printability criteria, in order to develop a printable paste without the need for trial-and-error printing tests. For instance, Zocca et al. [21] recommend a G'_{eq} value (*i.e.* G' in the linear viscoelastic region) between 10^5 and 10^6 Pa for a printable paste. Smay et al. [22] went further by providing a minimum value of G'_{eq} to print a scaffold without collapsing. The latter is defined as a function of the density of the paste and the geometric characteristics of the part. M'Barki et al. [23] did the same for the yield point value, by taking into account the effects of both gravity and capillary forces. However, Chan et al. [24] showed that the predictions of Smay et al. [22] and M'Barki et al. [23] did not always correspond to reality, especially in the case of high-density ceramic pastes. They have defined another criterion from their experiments, showing that the product of G'_{eq} and τ_y must exceed 5.10^6. Nevertheless, a printable boron carbide paste [25] was reported to have G'_{eq} and τ_y around 1000 and 120 Pa respectively, making their product much lower than the constant provided by Chan et al. These examples therefore show all the complexity of defining universal printability criteria [26].

Regarding rheological characterization in flow, when using a rotational rheometer, rupture occurs even at moderate shear rates for some formulations, despite their suitability for extrusion. This raises questions about the paste flow behaviour in classical capillary rheometry. Instead of undergoing simple shear (Poiseuille flow), plug flow is likely to occur with only a thin viscous layer on the walls. It is also important to note that a paste is a non-continuous medium, consisting of at least two phases: the mineral and organic phases. Therefore, theoretical approaches to flow are insufficient to fully understand their behaviour, as rheology characterizes only the macroscopic response of a paste sample.

Based on both oscillation and flow analyses, the present paper introduces ceramic pastes with higher values of rheological parameters than those typically reported in the literature. The latter often deviate from established printability maps [27,28]. This divergence arises from an aim to maximize solid loading while utilizing aqueous and eco-friendly systems.

Thus, it becomes evident that research should encompass factors beyond viscoelastic parameters, such as plasticity and phase segregation (*e.g.*, the filter-pressing phenomenon). If liquid phase migration occurs during extrusion, the composition and the rheological behaviour of the paste within the barrel may undergo continuous variations. This situation is particularly prone to occur when the paste flow is exceedingly slow, as noted by Liu et al. [29]. Such a phenomenon is identified as a source of defects in the final part [30]. In general, the water content of the paste, both before and after printing, significantly impacts its rheological behaviour. It is thus crucial to prevent the paste from drying out before its introduction into the reservoir and to control the drying kinetics after printing. Bio-based additives can play a substantial role in these aspects, particularly in terms of retaining water within the ceramic system. Indeed, they can serve as water retention agents, thereby assisting in preventing premature paste drying, which is crucial to maintain the appropriate paste rheology and ensure optimal printing performance.

The present paper focuses on the incorporation of environmentally friendly additives into concentrated aqueous alumina pastes (approaching 50 vol% solid loading). Particular attention was paid to the use of polymers not commonly employed in the ceramic field, such as polysaccharide gums (guar, psyllium) as binder. This study aims to (i) investigate the interactions between plant-based polymers and ceramic raw materials and (ii) optimize paste formulations for robocasting applications. Ultimately, unveiling printability criteria by comprehensively investigating the rheological properties, plasticity and cohesion of the pastes, paves the way to propose ready-to-use industrial-scale solutions.

2. Materials and methods

2.1. Raw materials

The ceramic paste formulation was carried out using alumina powder (P172SB, Alteo, France) as a reference material. Its specific surface area, measured from the B.E.T. method, is about 7.7 $m^2\ g^{-1}$ and its median particle size D50 is of 0.4 μm. Ammonium lignosulfonate (STARLIG AM®, LignoStar Group B.V., The Netherlands) was chosen as an eco-friendly dispersing agent. It is a harmless biological by-product in the traditional pulp processes, considered as the second most abundant natural polymer on Earth, after cellulose [31,32]. Its dispersion efficiency for alumina has been reported in a previous work by Marie et al. [33]. In comparison, ammonium polymethacrylate (Darvan® C–N, Vanderbilt Minerals LCC, USA) was also used as a reference dispersant [33].

Glycerol (Alfa Aesar A16205, Thermo Fisher GmbH, Germany) was used as a plasticizer. The latter is extracted from triglycerides naturally present in animal or vegetable fats such as olive, coconut or palm oils. For industrial purposes, it can also be synthesized.

The binder was introduced in the form of a physical gel, corresponding to an entanglement of polymer chains within a solvent. This gel was obtained by mixing in a planetary ball mill 5 wt% of a water-soluble polysaccharide powder with distilled water as a solvent. During this work, two natural polysaccharides were tested: psyllium (VITACEL® P95, J. Rettenmaier & Söhne, France) and guar gum (G4129, Sigma-Aldrich Chimie, France), that are both of plant origin [14,34,35]. Due to their high hydrophilic properties, psyllium and guar

gum are both able to form a gel-like network thanks to the swelling of their particles [36]. Furthermore, their ability to bind ceramic particles have already been demonstrated with a ceramic system [13] or manufacturing process [15] different from those reported in this work. Hence, their nontoxicity, their life cycle [14,35] and several properties (as thickening, stabilizing, gelling and/or binding [14,34] agents) make them interesting natural additives.

Oscillation and flow rheological analyses (see Appendix A in Supplementary data) conducted on psyllium and guar gum-based binders have confirmed their classification as gels. Furthermore, they have exhibited similar rheological characteristics, displaying a shear-thinning behaviour with a yield stress. Hence, they emerged as excellent candidates to replace traditional petrochemical-based binders in ceramic formulations.

2.2. Paste preparation

Alumina powder (noted A in the nomenclature of the pastes) was first pre-dispersed by mixing it with a dispersant – *i.e.* ammonium lignosulfonate (ALS) or Darvan® C–N (DCN) – and distilled water in a planetary ball mill for 1.5 h. Then, the slurry obtained was dried in an oven (100 °C) until the free water is completely removed. The resulting dried powder was crushed and sieved through a 200 μm mesh in order to limit the presence of residual agglomerates.

The mains focus of the upcoming study primarily explores two alumina pastes pre-dispersed with ALS: one utilizes P95 gel, while the other employs GG gel as a natural binder. Depending on the type of binder, a nomenclature has been introduced for these pastes: A-ALS-P95 for those based on psyllium and A-ALS-GG for those based on guar gum.

As part of this work, the reference paste formulation contains 49 vol % of alumina. The dispersant, polysaccharide and glycerol contents are respectively set at 1 wt%, 1.1 wt% and 3.9 wt% relative to the mass of alumina powder, according previous works [13,37]. The A-ALS-GG and A-ALS-P95 pastes contain 15.0 and 15.3 wt% of water relative to the mass of alumina, respectively.

As for the paste preparation protocol, the pre-dispersed alumina powder was introduced into a container with the glycerol (plasticizer) and the gel (binder), after achieving thermal equilibrium with the ambient conditions. Ceramic pastes were then made by mixing all these components at room temperature in a THINKY ARE-250 machine at 1000 rpm during three consecutive cycles, each lasting 3 min. After mixing, the paste was refrigerated at 4 °C for preservation. A minimum of 24 h of rest is preferred before using it in micro-extrusion.

2.3. Robocasting machine and printing conditions

Micro-extrusion of ceramic parts was performed by digitally controlling the movement of an in-house designed extrusion head. The latter is mounted on the platform of a CAD machine making it possible to move in X, Y and Z directions over a build tray. The printing paths were programmed with the computer language G-code which is read by the machine.

The paste was loaded into a 6 mm inner diameter barrel. The filament is deposited at a constant speed of 8 mm s^{-1}. The displacement of the plunger thus forces the flow of the paste through a 400 μm inner diameter nozzle, corresponding to a shear rate of 160 s^{-1}. In the present paper, the pastes under investigation display notably high viscosity, which is attributed to their high solid loading. Therefore, their extrusion through a narrow opening requires high extrusion pressures. Unlike commercial devices, the in-house developed extrusion head has the advantage of achieving extrusion pressures of up to several hundred bars.

The alumina parts are made in the form of scaffolds with a porous grid-like structure. This kind of architecture is commonly achieved for ceramic robocasting, especially in bio-printing, which enables a comparison with the literature [11,13,38]. In addition, it allows to evaluate printability in a simple and empirical way. Indeed, on the one hand, extrudability is checked from the continuous flow of the ceramic paste through the nozzle. On the other hand, the fidelity of the printed part with respect to the trajectory of the tool, is controlled by checking the periodic stacking of the layers and the shape retention of the filaments. The layer deposition paths were calculated for the design of scaffolds (10 × 10× 10 mm^3). The distance between the filaments is set at 0.8 mm, with an angular offset of 90° between two consecutive slices. The layer thickness is set at 320 μm, in order to compress the filaments by 20 % and promote their adhesion from one layer to another.

The environmental printing conditions were established and maintained constant using a climatic chamber that enclosed the robocasting machine. Parts were manufactured at room temperature (20–22 °C) with a high relative humidity between 65 and 75 %, in order to avoid possible defects due to poor partial drying conditions.

After printing, the alumina green parts were left to dry under room conditions (21 °C, 50 % relative humidity) for a minimum of 24 h before proceeding with the consolidation steps (*i.e.* debinding and sintering heat treatments).

2.4. Debinding and sintering heat treatments

After drying, alumina green parts were first heat treated in a muffle furnace (CT 9, Ceradel) for debinding at 500 °C (heating ramp: 1 °C.min^{-1}, dwell time: 1 h). The samples were subsequently sintered at 1580 °C (heating ramp: 5 °C.min^{-1}, dwell time: 4 h).

2.5. Characterization of polymers

2.5.1. Adsorption of the dispersant on the surface of alumina

A quartz crystal microbalance (QSense® QCM-D E4 Analyzer, Biolin Scientific) was used to collect information on the interactions between a polymer and a sensor. In particular, it allows to control the formation of a layer of polymer in solution on the surface of a sensor [39]. The latter is covered with a material whose surface simulates that of ceramic particles. As part of this work, alumina-coated quartz crystal sensors (QSense® QSX 309, Biolin Scientific) were used.

To allow good circulation of the solution through the analysis system and not to obstruct the capillaries of the measurement modules, the dispersant (either ALS or DCN) was diluted to a concentration of 0.5 g L^{-1}. Subsequently, the pH of the dispersant solution was adjusted to 8, matching the pH of the alumina pastes. Microbalance experiments were conducted to monitor the time-dependant changes in the thickness of ALS and DCN dispersants adsorbed onto the surface of the sensor.

2.5.2. Molecular weight of the polysaccharides

Size Exclusion Chromatography (SEC) is a technique based on the separation of macromolecules in solution, in the order of decreasing sizes. This method evaluates the molar mass M_i of each fraction eluted from a sample. Coupled with Multi-Angle Light Scattering (MALS), it provides information about the concentration c_i of each eluted fraction and overcomes many limitations of column calibration. SEC-MALS thus makes it possible to determine molar mass, polydispersity and radius of gyration of the macromolecules in solution [40].

SEC-MALS analyses were performed on natural polysaccharides, of which there is poor information in the literature. GG and P95 powders were diluted to 0.25 g L^{-1} in a 0.1 mol L^{-1} L_iNO_3 solution, which corresponds to the eluent of the SEC columns. The sample recovery (%) was evaluated as an indicator of the dissolution of the polymers in the eluent. It must be at least 70 % for the analyses to be representative.

2.5.3. Study of the aggregative nature of polysaccharides

The presence of proteins within polysaccharides is likely to induce an aggregation phenomenon. Hence, the protein content in both GG and P95 powders was determined through the Bradford assay [41]. The latter is based on a colorimetric reaction between Coomassie Brilliant

Blue dye and proteins in solution. The intensity of the resulting blue color, measured as the solution absorbance at 595 nm, is proportional to the protein concentration. This enables the quantification of protein content, considering a calibration curve established from solutions of known protein concentrations.

Bovine serum albumin (BSA) was used as a reference substance for the calibration. It was diluted in ultra-pure water at various concentrations ranging from 0.01 to 0.1 mg mL^{-1} to prepare a series of standard solutions, whose absorbance was measured at 595 nm. The resulting calibration curve [42] was then described by a Beer-Lambert law. After a linear regression (coefficient of determination R^2 of 0.9962), it corresponds to the following expression:

$$A = 0.0008 \times C \quad (1)$$

where A is the absorbance at 595 nm and C the protein concentration.

GG and P95 powders to be analysed were initially diluted to 1 mg mL^{-1} in ultra-pure water. The solutions were then placed in hemolysis tubes, to which 2.5 mL of Bradford reagent was added, followed by vortex mixing. The samples were kept in the dark for 5 min before measuring their absorbance at 595 nm, the wavelength at which absorption is proportional to the protein concentration according to Eq. (1).

2.6. Paste characterizations

2.6.1. Viscoelastic properties

The viscoelastic properties of the pastes were determined with a Discovery HR-2 rotational rheometer (TA Instruments) by using the oscillatory mode. This method allows a better understanding of the behaviour and structure of materials neither purely solid, nor purely liquid. It involves subjecting a material to a sinusoidal stress sweep and then measuring its strain.

The dynamic viscoelastic properties are characterized by the complex shear modulus G^* expressed by the following relation:

$$G^* = G' + iG'' \quad (2)$$

where G^* is composed of a real part G' called the storage (or elastic) modulus and an imaginary part G'' called the loss (or viscous) modulus [23]. The higher G^*, the more rigid the material.

Experiments were carried out by using a 4 mm diameter parallel plate with a 2000 μm gap size. The bottom plate temperature was controlled at 22 °C thanks to a Peltier plate. Moreover, each measurement was performed with a metal cover and distilled water as a solvent trap to prevent samples from drying out while testing. The linear viscoelastic region (LVER) was evaluated by an oscillatory stress sweep ranging from 0.2 to 2.10^5 Pa at a constant frequency set at 1 Hz.

The ageing of the pastes (see Appendix B in Supplementary data) was investigated by monitoring the evolution of their viscoelastic properties over time.

2.6.2. Capillary rheometry assembly on the extrusion head

Flow and oscillation analyses carried out by rotational rheometers are not necessarily suited to the description of ceramic bodies intended to be extruded. Capillary rheometry appears more adapted for the rheological study of a paste because its operating principle is close to robocasting conditions.

Classical capillary rheometry requires a large quantity of paste and the multiplication of analyses in order to be able to apply the Bagley [43], Mooney and Weißenberg-Rabinowitsch [44] corrections when dealing with non-Newtonian fluids. From a practical standpoint, setting up these analyses presents challenges, as it necessitates multiple reservoir fillings. Stresses may develop even before the experiment starts, potentially introducing air bubbles that disrupt measurements. This method is also likely to induce filter-pressing in the paste, altering its flow behaviour. Consequently, these challenges can result in measurement reproducibility issues and complicate the interpretation of classical capillary rheometry findings.

To overcome all these limitations, a capillary rheometry device was developed directly on the robocasting machine, in order to get as close as possible to robocasting conditions. A pressure sensor was installed on the extrusion head to measure the pressure drop. The volume flow is imposed by the speed of an extruder screw, controlling the movement of the plunger within the extrusion chamber. Three different capillaries were used at the outlet, with respective length-to-radius ratios of 8.3, 10.6 and 18.6. After verifying the reliability of the capillary rheometry device using standard formulations, the A-ALS-GG and A-ALS-P95 pastes were analysed by imposing decreasing shear rate values.

There are several models capable of describing the rheological behaviour of a fluid. A common representation involves plotting shear stress τ versus shear rate $\dot{\gamma}$ to create rheograms. Robocasting formulations are usually shear-thinning pasty fluids, with a minimum shear stress required to break their internal structure and initiate flow (yield stress). After applying the Bagley, Mooney and Weißenberg-Rabinowitsch corrections, the behaviour of the pastes was thus described by the Herschel-Bulkley model [45], which applies to pasty fluids such as:

$$\tau = \tau_s + k\dot{\gamma}^n \quad (3)$$

where τ_s is the yield stress, k is the consistency and n is the flow index.

2.7. Plastic limit and drying kinetics

Plasticity is usually defined by the ability of a material to deform irreversibly under a mechanical stress, without breaking. In this work, the plastic limit has been assessed from two methods.

Atterberg's work allowed defining a standardized test method to determine among others the plastic limit (PL) of fine-grained soils. The thread hand rolling procedure is described in the ASTM Designation D4318-17e1 [46]. It consists of hand rolling a homogeneous portion of material into a thread, between two flat and non-porous surfaces. The PL is defined as the water content (on a dry weight basis) at which the material thread starts to crumble when it is 3 mm in diameter, changing from a plastic state of consistency to a solid one.

However, the Atterberg method, originally designed for clay materials, is known to exhibit some limitations [47]. Consequently, shrinkage was simultaneously monitored alongside mass loss to determine the water content corresponding to the end of the linear section of the Bigot curve, denoted as EL (see Fig. 1). As the drying process progresses and shrinkage occurs, particles move closer until they establish contact with each other. The end of the linear segment (EL) of the Bigot curve corresponds to the initiation of grain-to-grain contacts. Given that water

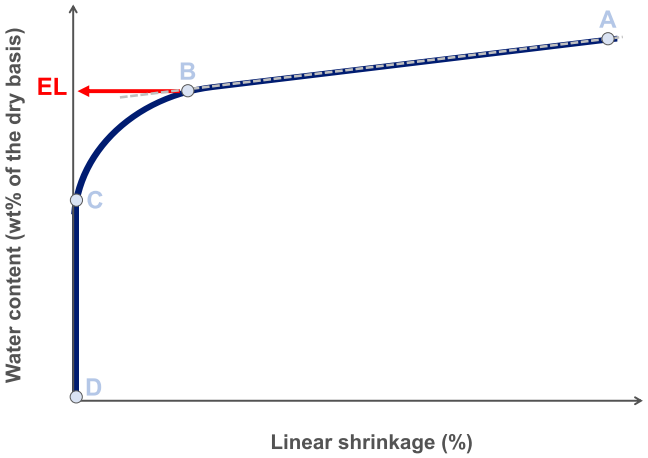

Fig. 1. Schematic representation of a typical Bigot curve.

initially contributes to plasticity by enveloping the particles, the EL point provides insights into the conclusion of the plastic domain. Kornmann [48] has noted that these two points, *i.e.*, PL from the Atterberg method and EL from the Bigot curve, are very close.

A Bigot device was set up to monitor the weight loss and the shrinkage in one direction of a paste sample over time. The primary objective of this experiment is to derive the Bigot curve from the collected data and subsequently determine the EL of a paste. The data are collected respectively by a precision scale (±1 mg) and by a laser distance sensor (±5 μm) placed above the sample. Both are connected to a computer, which allows data to be recorded throughout the drying process.

The A-ALS-GG and A-ALS-P95 pastes were analysed two days after their elaboration, to ensure they are in the same ageing conditions. Homogeneous paste samples were prepared so as to form a cube of about 20 mm square, according to the same method as Oummadi et al. [49]. To avoid their drying before the start of the analysis, each sample was kept 3 h in a chamber saturated with water vapor. Each measurement was performed under identical environmental conditions (20 °C and ambient relative humidity of about 40 %). Data were recorded during 48 h.

The Bigot curve is obtained by plotting the evolution of water content as a function of the linear shrinkage, both expressed on a dry basis [50]. Three main drying steps constitute the Bigot curve [48,51], as shown in Fig. 1.

During the first stage of drying (step A → B in Fig. 1), the water removal is balanced by a volumetric shrinkage: the height and weight of the paste sample decrease linearly as long as the pores are saturated with water. The EL point corresponds to the water content at the end of this stage, when the sample ceases to be plastic and begins to have a solid state of consistency [48,49]. The second drying stage (step B → C in Fig. 1) is characterized by a deceleration in shrinkage, as particles begin to come into contact. Shrinkage becomes negligible during the last drying stage (step C → D in Fig. 1); the sample's structure solidifies while its moisture content continues to decrease. At the end of drying, air has completely displaced the free water within the pores.

2.8. Quantification of the liquid phase migration

The ability of the paste to retain water was investigated under a shear rate similar to that applied in robocasting. The capillary rheometry assembly (see Section 2.6.2) was utilized to replicate the printing conditions, specifically the extrusion head equipped with a pressure sensor. An analysis was conducted by continuously monitoring the extrusion pressure over a 10-min duration, while keeping a constant shear rate ($\dot{\gamma} = 160\ s^{-1}$) within the chamber of the robocasting machine.

2.9. Characterization of the printed parts

2.9.1. Density measurements

Green density was geometrically calculated from the mass ratio to apparent solid volume of the dried samples.

The sintered scaffolds were also characterized for density according to Archimedes method described in the ASTM Designation B962-17 [52]. The relative density was calculated from the sintered density and the true density. The latter was measured with a helium pycnometer on a dried alumina powder sintered at 1580 °C.

2.9.2. Microstructural observation

The microstructure of the samples was studied using a scanning electron microscope (JSM-IT300, JEOL). It allowed observing the filaments, possible defects such as porosity or cracks, but also the grain arrangement and size after sintering. For the latter case, a thermal etching treatment (1530 °C, heating ramp: 20 °C/min, dwell time: 20 min) was conducted on a polished sample to reveal grain boundaries.

3. Results and discussions

3.1. Printability control of the pastes

Printability of the A-ALS-GG and A-ALS-P95 pastes was first evaluated by checking whether it was possible to print a scaffold by robocasting. Both alumina pastes were tested under the same conditions in order to establish a basis of comparison. These include aging of the pastes after elaboration, environmental conditions during printing and drying of the parts, but also parameters specific to both the machine and the layer deposition path. The resulting green parts are shown in Fig. 2.

Printability tests highlight different paste behaviour under the set robocasting conditions. It depends on the composition of the paste, in particular on the nature of the binder.

The A-ALS-GG paste extrudes well (Fig. 2a). When priming the nozzle, the paste flows properly, in a straight and continuous manner. Its flow stops when the plunger stops applying pressure. This leads to the manufacture of a 3D part faithful to the CAD model. The filaments exhibit good adhesion between two consecutive layers. They are also rigid enough to ensure excellent shape retention.

However, the A-ALS-P95 paste does not print well (see Fig. 2b and Fig. 2c). When priming the nozzle, it comes out in irregular waves. During printing, a liquid phase gradually appears in the thread of the nozzle, while the extrudates come out more and more stiff and dry. The part is weakened by cracked filaments which were caused by many discontinuities during printing.

The printability of both pastes differs under similar experimental conditions, even though they contain identical proportions of dispersant, binder, plasticizer and ceramic particles. The paste flow behaviour and the cohesion of the systems, in terms of water retention under shear, appear to be significantly influenced by the choice of binder. Consequently, a more comprehensive study of the gels and pastes was conducted, to gain a deeper understanding on how changes in additives can impact printability.

3.2. Characterization of the pastes at rest

3.2.1. Viscoelastic properties

The viscoelastic behaviour of both alumina pastes was studied through dynamic analyses in oscillatory mode with amplitude sweep, as shown in Fig. 3.

The A-ALS-GG and A-ALS-P95 pastes exhibit similar viscoelastic properties. They typically behave as an elastic solid ($G' > G''$) for a stress ranging from 150 and 6.10^3 Pa. In the LVER, the storage G' and loss G'' moduli are 1.10^8 and 2.10^7 Pa, respectively. After remaining constant in this linear region, they gradually decrease once the yield point τ_y is reached. The flow stress τ_f is approximately 4.10^4 Pa. The latter points out the transition to a viscous liquid-like behaviour ($G' < G''$).

Thanks to the ease of implementing amplitude sweep tests, the viscoelastic properties are commonly used in the literature to define "printability criteria", as mentioned in the introduction [21,22,24,26,53]. The reliability of the primary existing criteria was assessed using the data collected for both A-ALS-GG and A-ALS-P95 pastes. Based on these criteria, except for Zocca's [21], it is predicted that both pastes should be printable. However, as outlined in Section 3.1, one paste is printable (A-ALS-GG) while the other (A-ALS-P95) is not. This highlights the necessity of developing more reliable criteria, as well as characterization methods adept at discerning variations in paste printability.

3.2.2. Drying kinetics and plastic limit

Given that the printability issues of the A-ALS-P95 paste appear to stem from water retention problems under shear, particular attention was paid to the drying kinetics (see Fig. 4) and the plastic limit (denoted as PL and EL when obtained from Atterberg method and Bigot curve, respectively). Overall results are reported in Table 1.

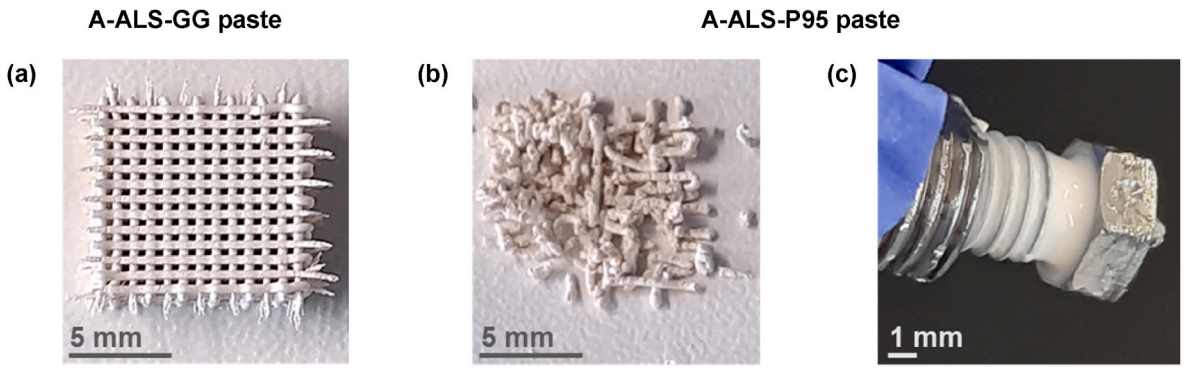

Fig. 2. Printability tests of the (a) A-ALS-GG and (b) A-ALS-P95 robocasting pastes, the latter (c) having filter-pressed during printing.

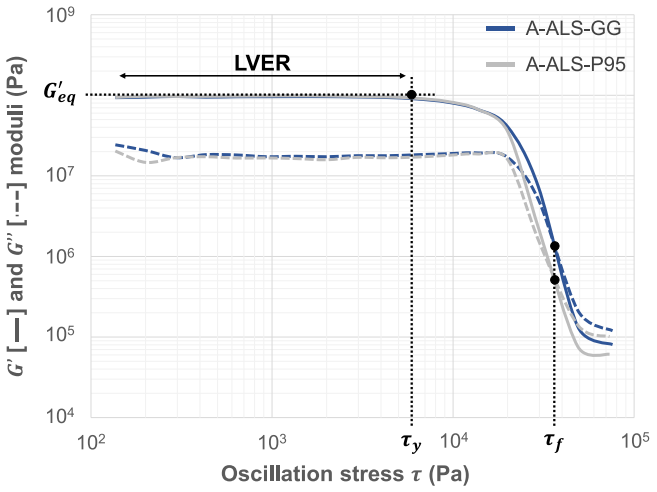

Fig. 3. Stress dependence of *G*' and *G*'' for the A-ALS-GG and A-ALS-P95 pastes.

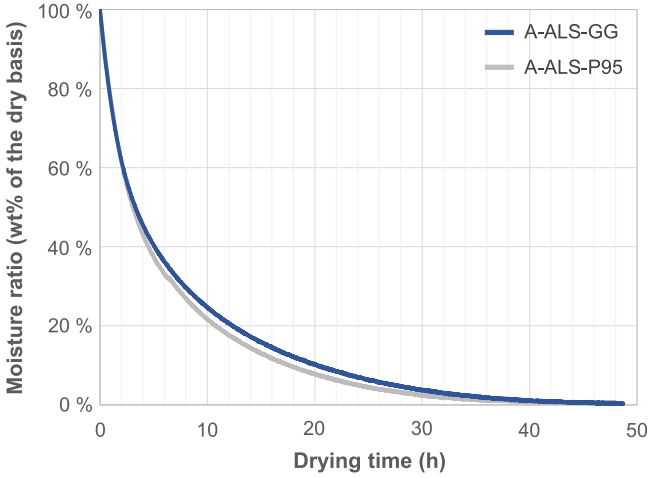

Fig. 4. Drying kinetics of the A-ALS-GG and A-ALS-P95 pastes.

The EL values of the A-ALS-GG paste obtained from the Bigot curve (16.4 wt%) is slightly higher than that of the A-ALS-P95 (15.2 wt%). The PL values obtained using the Atterberg method yield similar results (15.8 and 14.7 wt%, respectively), considering measurement uncertainties. Considering that the initial water content of both pastes is approximately 15 wt%, it can be concluded that their solid loading is indeed maximized.

Table 1
Plastic limit values (obtained from the Atterberg method and the Bigot curve) and duration of the first drying stage for both A-ALS-GG and A-ALS-P95 pastes.

	PL (Atterberg method)	EL (Bigot curve)	First drying stage
A-ALS-GG	15.8 ± 0.2 wt%	16.4 wt%	2–3 h
A-ALS-P95	14.7 ± 0.8 wt%	15.2 wt%	2–3 h

In the context of drying kinetics (see Fig. 4), the drying rate decreases as the drying process advances. The mass loss of both pastes became negligible after 40 h of drying. Fig. 4 also shows that the initial minutes of drying are critically important due to significant water loss. Therefore, special attention should be given to paste packaging (airtight) and minimizing handling time. Otherwise, considering the plastic limit values, water loss during the first drying stage may lead to a rapid transition from a plastic to a solid state.

In any case, the Bigot curve do not show any significant difference between the A-ALS-GG and A-ALS-P95 pastes, as their EL point and drying kinetics are similar. These data were collected while alumina pastes were at rest under ambient conditions; they are insufficient to characterize the pastes when subjected to high shear rates, as it might be during robocasting. Indeed, one can imagine that the nature of the binder influences the ability of a paste to retain water under extrusion conditions.

3.3. Flow behaviour of the pastes under high shear rates

Capillary rheometry tests were carried out as dynamic analyses in oscillatory mode did not detect any significant difference between the A-ALS-GG and A-ALS-P95 pastes. The behaviour of the pastes was thus

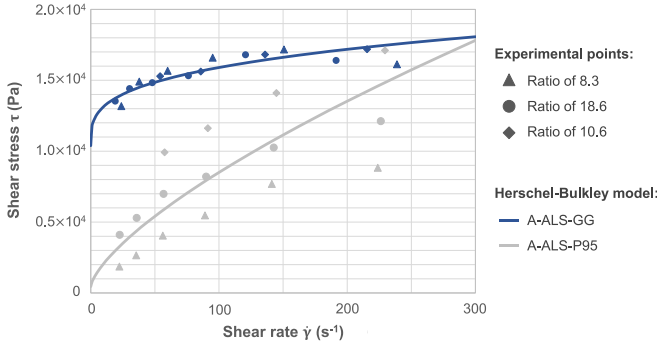

Fig. 5. Shear stress vs. shear rate of both A-ALS-GG and A-ALS-P95 pastes. Data were obtained from the capillary rheometry assembly installed on the extrusion head.

described in flow. Fig. 5 shows the rheograms of both alumina pastes, obtained after applying Bagley, Mooney and Weißenberg-Rabinowitsch corrections.

In Fig. 5, the experimental points (corresponding to the three different ratios of capillaries) are compared to the Herschel-Bulkley model. The latter allowed to identify the flow properties of each paste, given in Table 2.

In both cases, the experimental points show an increase in shear stress with shear rate. Although the measurements were carried out under the same conditions and repeated, the experimental points of the A-ALS-GG paste are much tighter around the Herschel-Bulkley model than those of the A-ALS-P95 one. This shows that the A-ALS-GG paste remains stable and homogeneous throughout the tests. However, as the analysis progresses with changing capillaries, the A-ALS-P95 paste exhibits less pronounced shear-thinning behaviour. Regarding this phenomenon, the data in Table 2 may be questionable because of the non-negligible difference that exists between the experimental points and the model.

According to Table 2, both pastes exhibit shear-thinning behaviour ($0 < n < 1$) with a yield stress ($\tau_s > 0$). In contrast to amplitude sweep tests (see Section 3.2.1), capillary rheometry reveals differences in the flow properties of the studied pastes. The A-ALS-P95 paste exhibits lower τ_s and k values compared to the A-ALS-GG paste, while its flow behaviour index n is higher. The low flow index value of the A-ALS-GG paste suggests possible plug flow behaviour, warranting further investigation under pressure conditions. Nevertheless, as discussed in Section 3.1., the A-ALS-GG paste flows better through a nozzle than the A-ALS-P95 paste, the latter being not printable under the same conditions. Thereby, a phenomenon potentially linked to the evolution of the A-ALS-P95 system during extrusion may be responsible for its non-printability. Consequently, the ability of the pastes to retain water under shear conditions of robocasting was further investigated.

3.4. Correlation between printing parameters and liquid phase migration

The ability of the pastes to retain water under shear conditions was assessed using pressure tests conducted with the capillary rheometry setup directly connected to the extrusion head of the robocasting machine. Fig. 6 shows the extrusion pressure profiles as a function of the time at $\dot{\gamma} = 160\ s^{-1}$. In the first few seconds of the test, the extrusion pressure continuously rises while priming the nozzle. However, once the pastes flow, two different scenarios occur.

Regarding the A-ALS-GG paste, the extrusion pressure stabilizes around 8 bars and remains constant all during the test. It drops after 10 min, when the experiment ends and the plunger ceases to exert pressure on the paste. This behaviour is typically that of a homogeneous paste whose composition does not vary during extrusion.

Regarding the A-ALS-P95 paste, the extrusion pressure gradually increases as the plunger moves. It reaches almost 40 bars, a value clearly higher than that necessary to force the flow of the A-ALS-GG paste.

Alongside liquid phase migration measurements, extruded filaments were sampled from the nozzle outlet to measure their water content. This allowed to determine whether this value changed during extrusion and how it related to the states of consistency, as indicated by the plastic limits reported in Table 1. In both cases, at the start of the test, the water content of the filaments exceeded the plastic limit of the pastes, indicating that they were in a plastic state of consistency.

The water content of the A-ALS-GG extruded filaments remained stable (14.9–15.0 wt%) during the test, confirming the stability and the homogeneity of this paste under robocasting conditions.

Table 2
Flow properties of the A-ALS-GG and A-ALS-P95 pastes, identified from the Herschel-Bulkley model.

	Yield shear stress τ_s (Pa)	Consistency k (Pa.s^n)	Flow index n
A-ALS-GG	1.0×10^5	1.3×10^4	0.30
A-ALS-P95	4.5×10^3	3.2×10^3	0.70

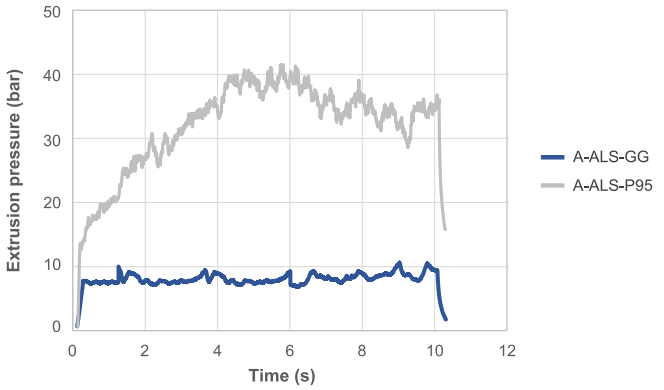

Fig. 6. Time dependence of the extrusion pressure as the plunger moves at constant speed ($\dot{\gamma} = 160\ s^{-1}$) through the reservoir to force the flow of the A-ALS-GG and A-ALS-P95 pastes.

However, the water content of the A-ALS-P95 extruded filaments decreased from 15.3 to 11.8 wt%. Comparing these data with those presented in Table 1 reveals that A-ALS-P95 paste changes from a plastic state of consistency to a solid one during extrusion. This paste thus undergoes a shift towards an increased dryness. As a result of filter-pressing, it becomes progressively more challenging to extrude (Fig. 6), explaining the disparity of the experimental points in Fig. 5 as well as the printability issues described in Section 3.1.

Therefore, this study has highlighted water retention in the paste under robocasting conditions as a crucial experimental criterion for printability. Additionally, it enabled real-time detection of a common extrusion issue: the migration of the liquid phase. These measurements, conducted directly at the nozzle inlet of the extrusion head during printing, hold promise for broader adoption in assessing the printability of various pastes in the future. Furthermore, machine learning approaches could potentially facilitate real-time adjustments to either printing conditions or formulation. However, the latter requires a more in-depth understanding of the underlying mechanisms governing printability at the level of paste components.

3.5. Better understanding printability through the study of paste components

3.5.1. Organization of the dispersant around alumina particles

In-depth characterization of both alumina pastes revealed the macroscopic reason why one paste (A-ALS-GG) prints while the other (A-ALS-P95) does not. However, this does not quantify the impact of the binder change or explain why filter-pressing occurs in the P95-based paste but not in the GG-based. To gain a deeper understanding of printability and insights for direct formulation adjustments, particular attention was paid to the paste components and their interactions around the alumina particles.

On the one hand, the minimum distance d between two adjacent alumina particles was estimated, by making an analogy with the hard spheres model. By assimilating alumina particles to spheres, this assumes that each grain is spherical, of constant radius and density. In theory, when d is zero, the maximum solid volume fraction Φ_{max} is 0.74 for a classical compact structure, such as the face-centered cubic (fcc) one, for which a unit cell is modeled in Fig. 7.

Regarding ceramic pastes, the maximum solid volume fraction Φ is much lower than 0.74; it corresponds to the alumina solid loading, *i.e.* about 0.49 in this work. Unlike theoretical close packed structures, the surface of two adjacent alumina particles would not be in direct contact, but separated by a layer of minimum thickness $d/2$. The latter,

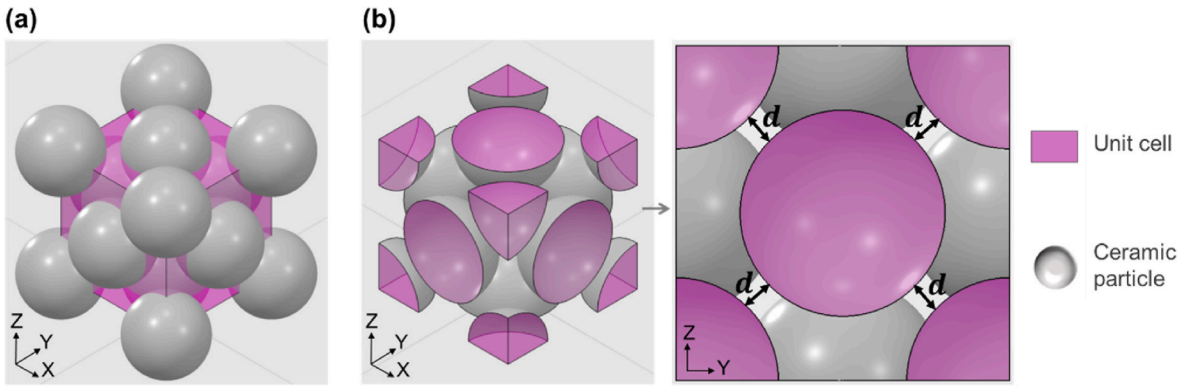

Fig. 7. CAD modeling (a) of a fcc compact structure and (b) of the spheres occupying the unit cell volume, to assess the solid volume fraction as a function of the inter-particle distance *d*.

corresponding to an interstitial fluid surrounding each particle, can be expressed as:

$$d = 2R\left[\left(\frac{\Phi}{\Phi_{max}}\right)^{-1/3} - 1\right] \quad (4)$$

where R is the mean radius of alumina particles. The numerical application thus estimated d at 59.5 nm for A-ALS-GG and A-ALS-P95 pastes. This value was confirmed from a CAD software, by plotting the evolution of Φ as a function of d, the latter being defined as an input variable. The findings shown in Fig. 8 align with those obtained from Eq. (4).

On the other hand, the dispersant adsorption on the alumina surface was examined using a quartz crystal microbalance. In addition to confirming the affinity between alumina and the ALS dispersant, it revealed that the layer thickness of the latter was about 40 nm on the surface of the particles. By comparing this value to d, it indicates overlapping zones occupied by the dispersant between adjacent alumina particles.

Consequently, the interstitial fluid surrounding alumina particles is already occupied by the dispersant. It is assumed that the steric hindrance and/or the interactions (such as chain entanglement or bonding) of other components (binder, plasticizer) within this fluid will impact the reorientation of polymer chains under shear and, subsequently, the paste flow behaviour during robocasting.

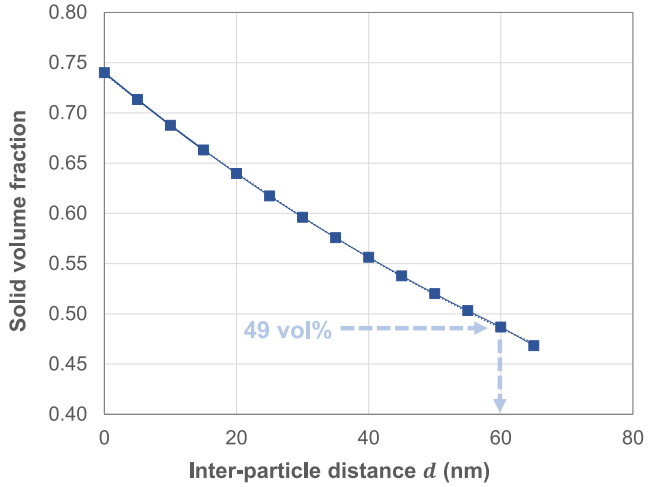

Fig. 8. Solid volume fraction Φ vs. inter-particle distance d between two adjacent alumina particles, for which the medium particle size D_{50} equals 400 nm.

3.5.2. *Steric hindrance of the polymers within the interstitial fluid*

In addition to the dispersant, the interstitial fluid consists of a binder (GG or P95 gel) and a plasticizer (glycerol). At the formulation level, the only difference between the A-ALS-GG and A-ALS-P95 pastes lies in the nature of the binder, since the glycerol is introduced in the same proportions. Attention has been paid to an in-depth characterization of the natural polymers GG and P95, about which there is poor information in the literature. It is assumed that a greater steric hindrance of P95 than that of GG hampers paste flow; this would explain the lack of cohesion and the filter-pressing of the A-ALS-P95 paste observed during printing.

Data obtained from SEC-MALS analyses on both raw powder and gel of GG and P95 polymers are given in Table 3.

SEC-MALS analyses obtained for GG show similar data between the raw powder and the gel, which means that preparing the gel in a planetary ball mill does not break the polymer chains. However, the sample recovery is only of 33 % for P95, due to sample losses during filtration upstream of the SEC columns. Thus, it is assumed that P95 aggregates in the $LiNO_3$ eluent. As a result, the collected data for P95 only pertain to fractions smaller in size than the filter porosity (0.45 μm), and, by extension, to the less aggregative fractions.

The aggregative nature of P95 may be linked to the reduced water retention observed on the A-ALS-P95 paste under the shear conditions of robocasting.

The presence of micro-aggregates could be attributed to various interactions among polysaccharides and/or other constituents in the extracted powder source. For instance, hydrogen bonds and hydrophobic interactions may offer plausible explanations for this aggregative behaviour. Moreover, the presence of proteins is a known factor that can lead to strong associations and induce aggregation. Consequently, a Bradford assay [41] was conducted on both GG and P95 powders to further investigate this phenomenon. Results are reported in Table 4.

This colorimetric protein assay determined a negligible protein content in GG (less than 1 wt%), compared to 3.6 wt% in P95. Hence, the P95 gel contains impurities which could be in the form of micro-aggregates, within the entanglement of the polymer chains.

It is assumed that the micro-aggregates add steric hindrance in the interstitial fluid surrounding the alumina particles of the A-ALS-P95 paste, compared to that of A-ALS-GG. This can affect the mobility of the components under high shear rates, especially between two alumina

Table 3
Number and weight average molar masses and sample recovery rate obtained by SEC-MALS analyses made on GG and P95 polymers.

	$\overline{M}_n$ (kg.mol^{-1})	$\overline{M}_w$ (kg.mol^{-1})	Sample recovery (%)
GG (powder)	1.9×10^3	1.9×10^3	71
GG (gel)	1.9×10^3	1.9×10^3	70
P95 (powder)	0.5×10^3	1.5×10^3	33

Table 4
Protein quantification in GG and P95 polysaccharides using the Bradford method.

	A	*C* (µg of proteins per 1 mg of sample)	Protein content (wt %)
GG (powder)	0.008	< 10	< 1.0
P95 (powder)	0.029	36	3.6

particles, where $\dot{\gamma}$ is maximum. A schematic representation is given in Fig. 9, depending on the nature of the binder. The reorientation of the polymer chains under robocasting conditions is also shown.

According to Fig. 9 a, it is assumed that the polymers reorient under the shear effect, which allows the A-ALS-GG paste to flow homogeneously. However, the micro-aggregates present in the A-ALS-P95 paste reduce the mobility of the components, and therefore the reorientation of the polymer chains (Fig. 9 b). One can infer that under shear, only the solvent is able to move. Hence, this explains the liquid phase migration observed while printing the A-ALS-P95 paste.

3.6. Some solutions to improve the printability of a paste

In the preceding section, the comprehensive study of the paste components and their interactions has provided insights into some correlations between formulation and printability.

To validate the substantial role of polymer steric hindrance within the interstitial fluid, efforts focused on making a P95-based paste printable under the robocasting conditions established for this study. In this example, two scenarios have been considered to improve the reorientation of polymers under high shear rates and increase the mobility of the components.

The first possibility consists in reducing the presence of micro-aggregates within the P95 gel. An A-ALS-P95 paste was formulated as described in Section 2.2, but introducing a less concentrated gel, containing 3 wt% of P95 powder instead of the previous 5 wt%.

By keeping a P95 gel concentrated at 5 wt% by weight, another source of improvement lies on using a less steric dispersant than ALS. A study on the dispersion of alumina showed that an ammonium polymethacrylate dispersant (or DCN for Darvan® C–N) had a dispersing power similar to that of ALS [48]. Unlike ALS, which is rather steric due to the large number of cycles in its structure, DCN corresponds to a rather linear polymer chain and has a preponderant electrostatic effect. An analysis carried out with a quartz crystal microbalance confirmed that the layer thickness of the DCN dispersant, adsorbed on the surface of alumina particles was lower than that of ALS; it is indeed of 6 nm, compared to 40 nm for ALS. In contrast to the previous cases, this time there is no overlap of the zones occupied by the DCN dispersant, even at the minimal inter-particle distance *d* (60 nm). This results in the interstitial fluid surrounding the alumina particles being less congested for the A-DCN-P95 paste compared to the A-ALS-P95 paste. It is also assumed that there is less entanglement between the dispersant and the rest of the polymers, as the DCN polymer chains wrap more tightly around the particles.

Printability tests were conducted for these two scenarios under the same robocasting conditions as those detailed in Section 3.1: the A-ALS-P95 paste with a 3 wt% gel (referred to as A-ALS-P95(3) paste) and the A-DCN-P95 paste. In both cases, a noticeable improvement is evident, as both P95-based pastes become printable and enable the construction of grid-like scaffolds.

Fig. 10 illustrates pressure measurements, demonstrating enhanced printability in the novel P95-based pastes due to reduced filter-pressing.

In contrast to the initial A-ALS-P95 paste, which exhibited gradual

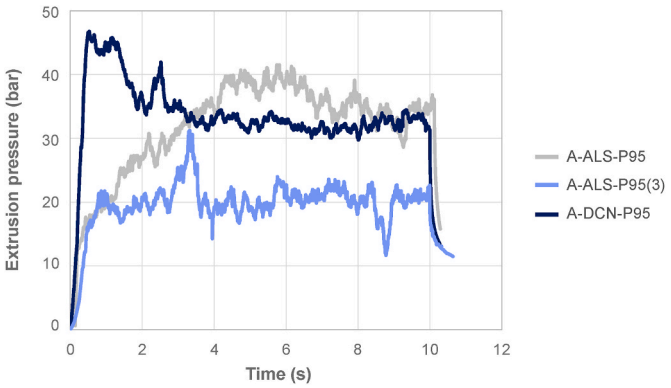

Fig. 10. Measurement of liquid phase migration over time through the analysis of extrusion pressure in improved P95-based pastes, in comparison to the initial A-ALS-P95.

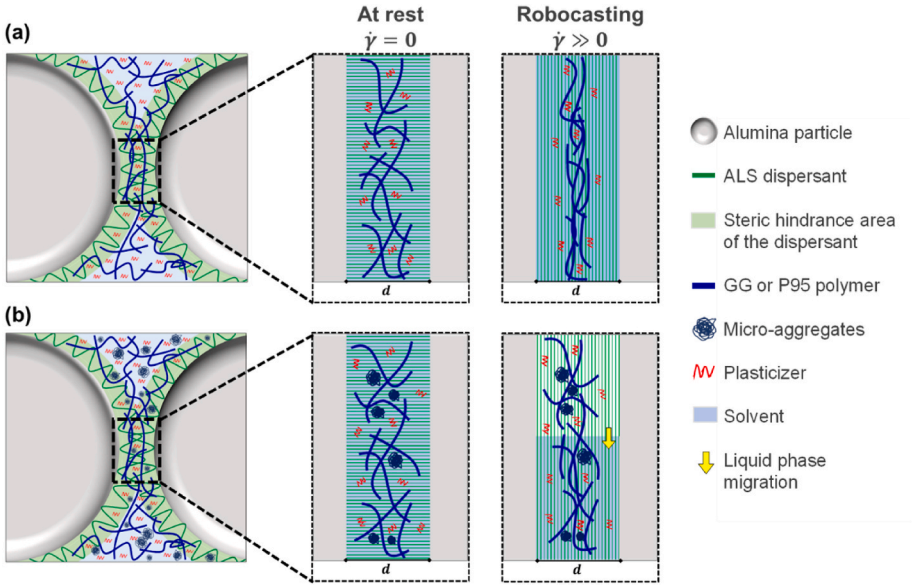

Fig. 9. Schematic representation of the organization of the components between two alumina particles and their mobility during extrusion of (a) A-ALS-GG and (b) A-ALS-P95 pastes.

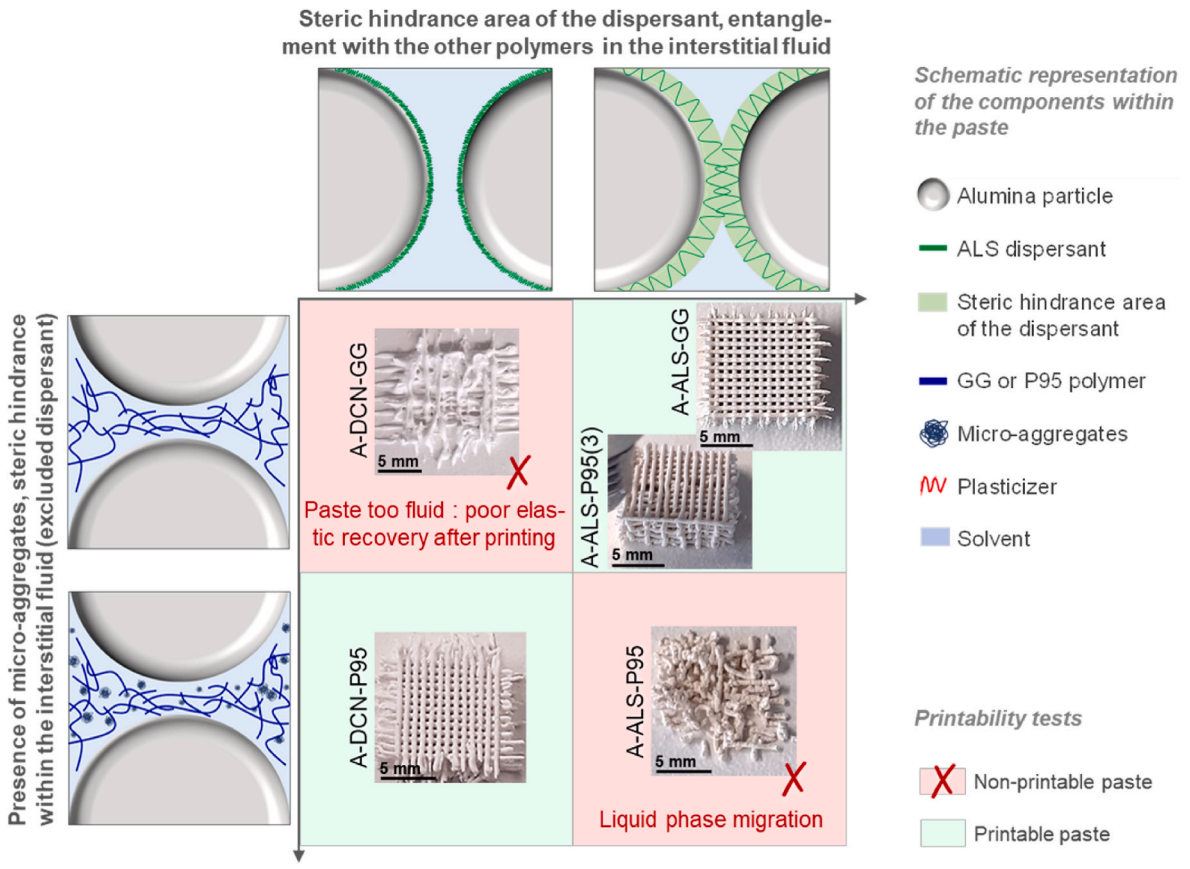

Fig. 11. Synthesis diagram showing the correlations between paste formulations and their printability under the same robocasting conditions, assuming that the amounts of alumina and plasticizer are identical.

and unstable extrusion pressure throughout the test, the new pastes display a distinct behaviour. Upon nozzle initiation, extrusion pressure rapidly increases and then stabilizes at average values. Extrusion pressures for A-ALS-P95(3) and A-DCN-P95 pastes are approximately 20 and 32 bars, well within the capacity of our in-house robocasting machine, capable of handling pressures of several hundred bars. It is worth noting, however, that minor irregularities are observed, possibly linked to agglomerates. In any case, despite the need for further optimization, a significant improvement over the A-ALS-P95 paste is evident, aligning with the theoretical framework of this paper. Thus, precise control of polymer steric hindrance and interactions remains essential to minimize liquid phase migration under shear.

A synthesis diagram is shown in Fig. 11 to summarize the printability of all the studied eco-friendly formulations.

This study underscored the importance of focusing on the interactions among all the components of a robocasting paste. All tested formulations have highlighted the necessity for striking a compromise between polymer steric hindrance (both in the interstitial fluid and on the alumina surface) and the strength of the interactions among polymers themselves and/or with alumina. If these two criteria are too low, the paste may exhibit excessive fluidity under identical robocasting conditions, resulting in poor elastic recovery after printing and the collapse of the part (as seen for the A-DCN-GG paste in Fig. 11). While further optimization of P95-based formulations is required, in particular to reinforce the mechanical strength of green bodies, these tests have provided valuable insights for improving printability.

3.7. Final properties of sintered parts

Beyond studying printability, this work led to the 3D printing of totally eco-responsible robocasting pastes. Typical scaffolds obtained after sintering from the A-ALS-GG paste are shown in Fig. 12.

In addition to excellent shape fidelity compared to the CAD model, the sintered scaffolds exhibit similar properties to alumina parts obtained with conventional formulations: grains of 3.7 μm on average, 98 % relative density for the solid skeleton and 17 % of shrinkage after sintering [54].

Dense parts printed from this A-ALS-GG paste were mechanically tested and yielded results comparable to those reported in the literature for conventional alumina-based formulations. The experimental characterization procedure is outlined in previous work through 4-point bending tests and ultrasonic testing [55]. Fig. 13 provides an example of a response curve from a 4-point bending test conducted on one of the ten tested samples. A typical brittle behavior of an alumina piece is

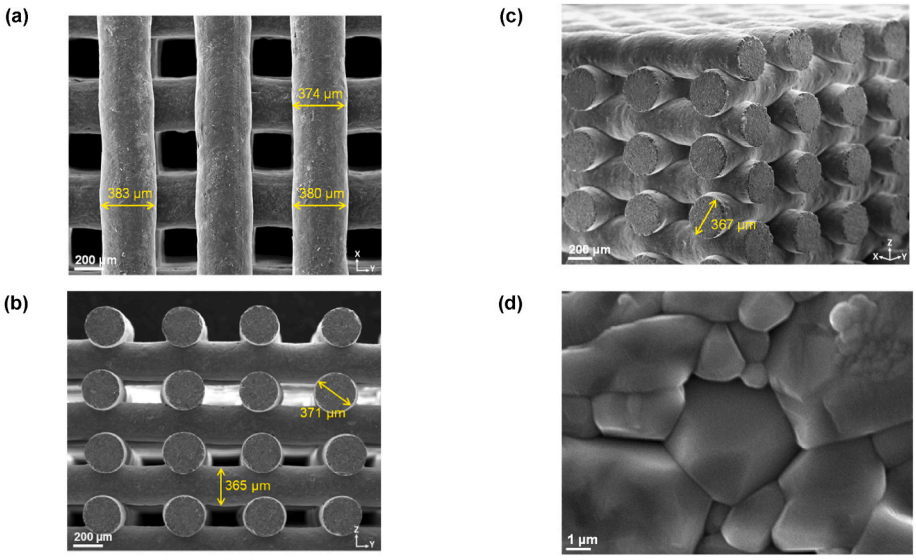

Fig. 12. SEM micrographs of alumina scaffolds sintered at 1580 °C: (a) top and (b) (c) side views of the grid-like pattern, and (d) morphology and arrangement of the grains.

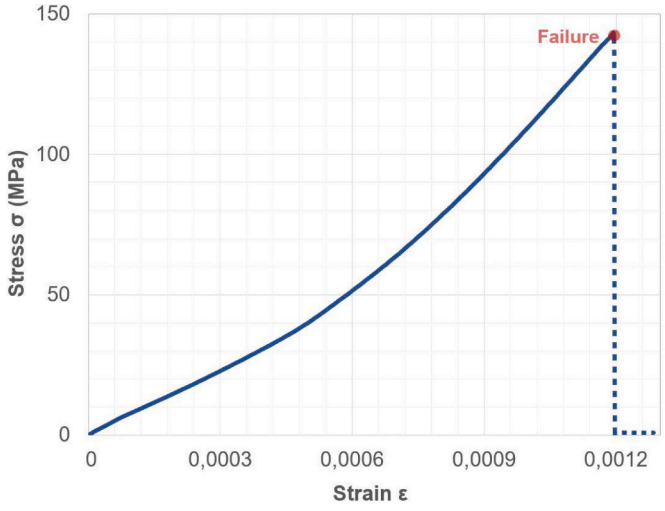

Fig. 13. Evolution of the stress as a function of strain for a dense part printed from a A-ALS-GG paste during a four-point bending test.

clearly identified. In particular, the synthesis of the test campaign results highlights a sample exhibiting a Young's modulus of 355 GPa, a Poisson's ratio of 0.23 and a flexural strength of 140 MPa [37,42] (Fig. 13.). Therefore, this confirms the promising potential of using natural additives for industrial applications.

4. Conclusions

Valuable insights were provided into the mechanisms governing the printability of pastes intended for the robocasting process. The rheological characteristics, as well as other properties relatively underreported in the literature, including plasticity and paste water retention under shear, have been assessed and correlated with printability.

Findings suggest that while characterizing the viscoelastic properties of pastes is necessary, it is largely insufficient to distinguish a printable paste (A-ALS-GG) from a non-printable one (A-ALS-P95). Traditional analyses conducted with rotational rheometers do not adequately capture the behaviour of pastes subjected to high shear stresses, such as those experienced during extrusion. This highlights the limitations of existing printability criteria reported in the literature, which may not be reliably applicable to the robocasting process. To gain a deeper understanding of paste flow behaviour under conditions approaching those of robocasting, it is essential to consider alternative means of characterization.

The properties of both the pastes and their components have been correlated to the concept of printability. This work demonstrates that the organization and interactions among polymer chains of binders, plasticizers and dispersants around ceramic particles, as well as their ability to move and reorient under high shear stresses, strongly affect the paste behaviour at various stages of printing: (i) the initiation of flow, (ii) the homogeneity and viscosity during the extrusion and (iii) the cohesion between the mineral (ceramic particles) and organic (interstitial fluid) phases.

In this respect, controlling liquid phase migration under high shear stresses emerged as a crucial criterion for the good progress of the robocasting process. A novel method for testing printability has been developed to observe and quantify, at the nozzle inlet, the segregation of the mineral phase under the pressure applied by the plunger during extrusion.

The focus on eco-friendly paste formulations has highlighted the importance of mastering the mechanisms that govern printability in robocasting. In the future, printability criteria could integrate factors like steric hindrance and polymer interactions in the interstitial fluid surrounding ceramic particles through numerical approaches. This would potentially enhance the development of ready-to-use feedstock for robocasting, particularly when replacing traditional petrochemical additives with plant-based polymers. Indeed, additives of natural origin

may exhibit composition or purity variability from one batch to another, which could impact paste flow behaviour. From an industrial perspective, the use of machine learning holds promise for real-time adjustments to paste formulation or shear rates during robocasting. This approach would mitigate fluctuations in the properties of natural additives, ensuring 3D printing of eco-friendly ceramic parts and advancing towards a more sustainable industry.

CRediT authorship contribution statement

Delphine Gourdonnaud: Investigation, Writing – original draft, Writing – review & editing, Visualization, Validation. **Julie Bourret:** Conceptualization, Methodology, Validation, Investigation, Writing – original draft, Writing – review & editing, Supervision, Visualization, Project administration. **Vincent Pateloup:** Conceptualization, Methodology, Software, Validation, Investigation, Writing – original draft, Supervision, Project administration. **Lisa Giardi:** Investigation, Validation, Visualization. **Luc Picton:** Conceptualization, Validation, Investigation, Resources, Writing – original draft, Writing – review & editing. **Vincent Chaleix:** Conceptualization, Validation. **Thierry Chartier:** Conceptualization, Methodology, Resources. **Benoit Naït-Ali:** Methodology, Investigation. **Marguerite Bienia:** Methodology, Investigation. **Pierre-Marie Geffroy:** Conceptualization, Validation, Investigation, Writing – original draft, Writing – review & editing, Supervision, Project administration.

Declaration of competing interest

The authors declare that they have no known competing financial interests or personal relationships that could have appeared to influence the work reported in this paper.

Acknowledgements

The authors would like to sincerely thank Christophe Rihouey for his help in carrying out the SEC-MALS analyses described in this paper and the Nouvelle-Aquitaine region for providing financial support.

Appendix A. Rheological properties of the polysaccharide binders

Psyllium and guar gum are plant-derived polysaccharides. In powdered form, their particles have the unique property of swelling upon contact with water, forming a gel-like network. This characteristic makes them excellent candidates to serve as binders and promote cohesion in the green state of ceramic parts printed by robocasting.

A1. Methods for the rheological characterization of psyllium (P95) and guar gum (GG) gels used as binders

A1.1. Definition of a gel

A gel corresponds to a three-dimensional network of molecular chains dispersed in a solvent. From a polymer perspective [56], a gel is defined based on three main criteria, namely:

- Containing at least 95 wt% of the solvent.
- Having a decade difference between the storage (G') and the loss (G'') moduli, at a given frequency.
- Demonstrating stability in the storage (G') and the loss (G'') moduli with frequency, across a given range of frequencies.

A1.2. Viscoelastic properties of binders

The viscoelastic properties of GG and P95 binders determined with a Discovery HR-2 Rheometer (TA Instruments) by using the oscillatory mode.

Amplitude sweep tests were carried out by using a 4 mm diameter parallel plate with a 2000 μm gap size. The temperature was controlled at 22 °C thanks to a Peltier plate Steel. Moreover, each measurement was performed with a metal cover and distilled water as a solvent trap to prevent samples from drying out while testing. The linear viscoelastic region was evaluated by an oscillatory stress sweep ranging from 0.2 to 2.10^5 Pa at a constant frequency set at 1 Hz.

Frequency sweep tests were performed from 0.1 to 100 Hz at a constant oscillation amplitude stress. The latter is chosen in the middle of the LVER, as determined from amplitude sweep tests. In the present study, analyses were conducted at 75 Pa.

A1.3. Flow properties of binders

The flow properties of binders were studied using the rotational Discovery H-R2 Rheometer. A flow sweep test provided insights into the viscosity and flow behaviour of the gels under controlled rotational conditions.

Experiments were carried out by using a 40 mm diameter 4° cone plate. Temperature was set at 22 °C, the latter being controlled by a Peltier plate Steel, and each experiment was carried out under a metal cover to limit drying of the binders. Viscosity and shear stress were measured as a function of shear rate, for values ranging from 0.1 to 200 s^{-1}.

A2. Rheological characterization of the binders

A2.1. Verification of the criteria to define a gel

Rheological analyses were carried out in oscillation to ensure that the aqueous mixtures of polysaccharides correspond to gels. As a reminder, these mixtures correspond to 5 wt% of polysaccharide powder and 95 wt% of water.

Similar data having been obtained with psyllium (see Section A2.2), only the results concerning guar gum are displayed in Fig. A-1.

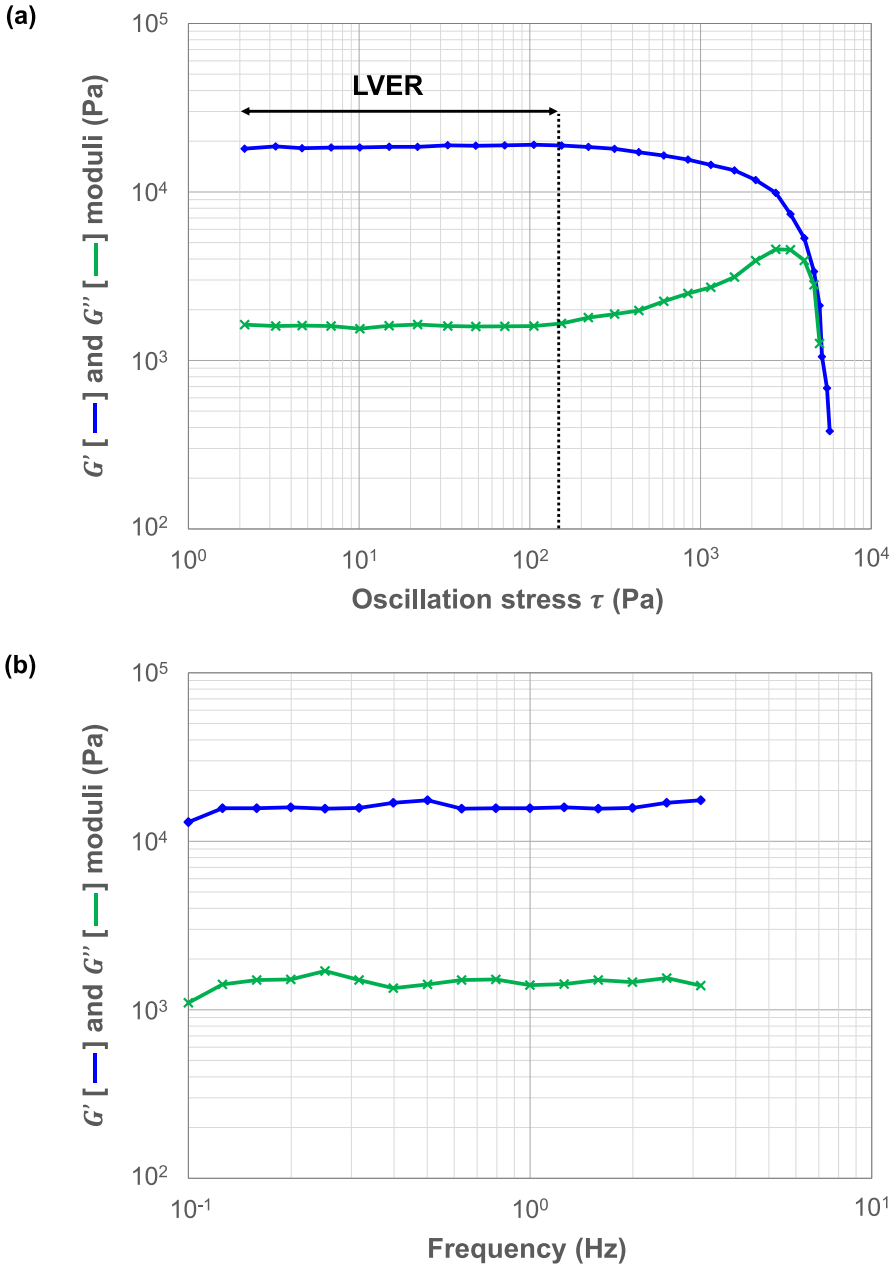

Fig. A-1. Viscoelastic properties of the aqueous mixture of guar gum: (a) amplitude and (b) frequency sweep tests.

According to Fig. A-1 a, the linear viscoelastic region (LVER) is defined in a range of oscillatory stresses ranging from 2 to approximately 150 Pa. In this range, the storage (G') and the loss (G'') moduli are approximately 2.10^4 and 1.10^3 Pa, respectively.

Fig. A-1 b shows that G' and G'' remain relatively stable over a frequency range extending from 0.1 to approximately 3 Hz. On average, they are approximately $1.6.10^4$ Pa and $1.5.10^3$ Pa, respectively, which coincides with the values obtained from Fig. A-1 a. Beyond this frequency range, the system begins to lose structure and starts to flow, making the collected data unusable.

These two analyses conducted under the oscillation mode have thus highlighted that the viscoelastic moduli differ by at least a decade. Furthermore, G' and G'' are independent of the oscillation frequency over a certain frequency range, ranging from 0.1 to 3 Hz. Considering that the polysaccharide mixture contains 95 wt% of solvent, the three criteria mentioned in Section 1.1. are met. This confirms that the aqueous mixtures of polysaccharides are gels.

A2.2. Rheological behaviour of GG and P95 gels

The rheological properties of both GG and P95 gels were studied through oscillatory stress sweep and flow sweep tests. Results are shown in Fig. A-2.

According to Fig. A-1, both GG and P95 gel exhibit similar viscoelastic properties, with a LVER defined between 2 and 150 Pa, approximately. In this range of oscillatory stresses, G' and G'' moduli are about $1\text{-}2.10^4$ and 1.10^3 Pa, respectively.

According to Fig. A-2, both gels exhibit a shear thinning behaviour with a yield stress. Indeed, as the shear rate increases, the viscosity decreases,

and it begins to stabilize at around 2–3 Pa s at a shear rate of 150 s^{-1}.

The yield stresses of the GG and P95 gels are quite close, i.e. 17 and 23 Pa, respectively. For high shear rates, the viscosity of P95 gel is higher than that of GG gel, even though both gels have the same mass fraction of polysaccharide powder. This slight difference between both gels could be explained by the aggregation phenomenon present psyllium (as discussed in Section 3.6.2 of the main article). In fact, the P95 gel may not be just a simple entanglement of polymer chains, as for GG gel. Instead, it appears to have a structure with micro-aggregates (comprising proteins) distributed within the entanglement of polymer chains.

Therefore, the presence of micro-aggregates within psyllium is likely to restrict the movement of polymer chains. This would explain why a higher yield stress than that of guar gum is required to initiate flow and also why the P95 gel is more viscous.

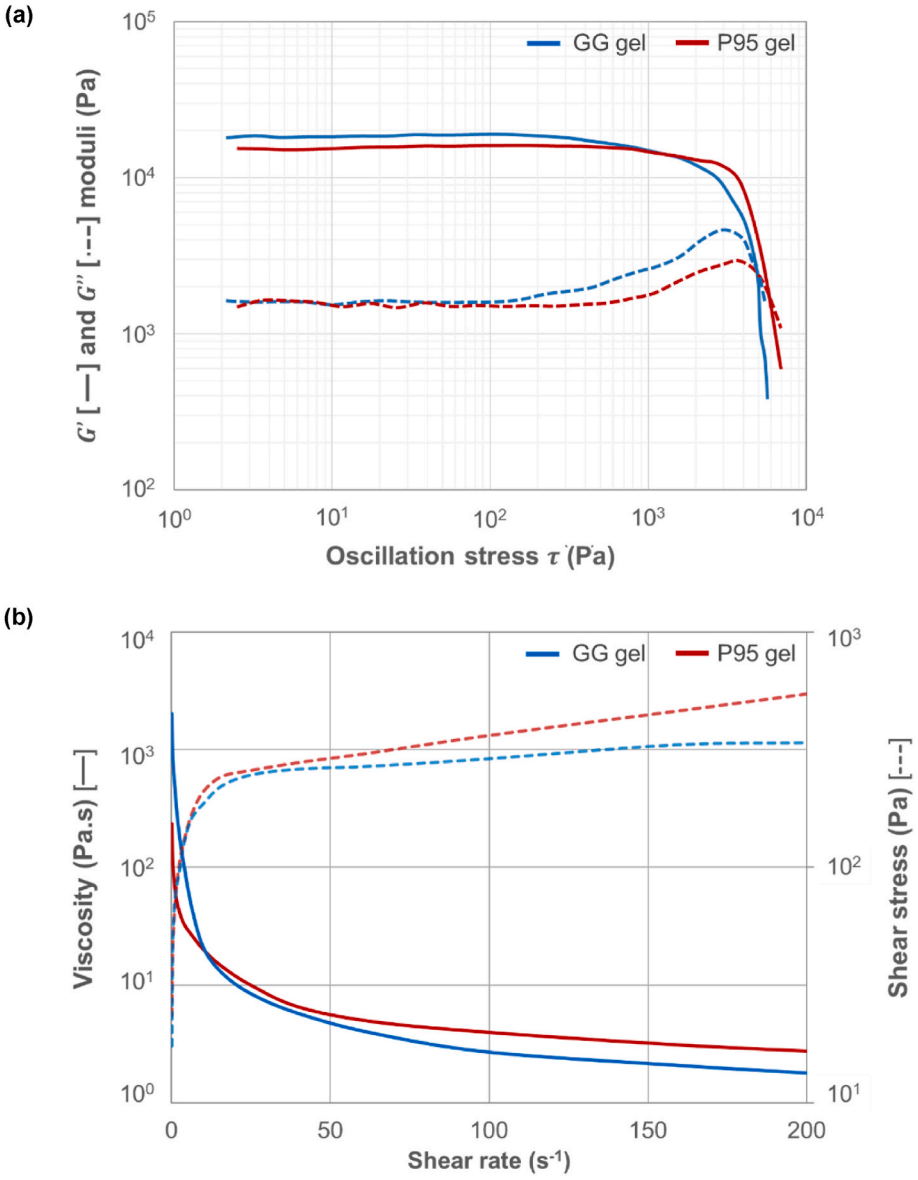

Fig. A-2. Rheological characterizations of the GG and P95 gels: (a) amplitude sweep test and (b) flow behaviour.

Although their characteristics vary slightly according to Fig. A-2, both GG and P95 gels exhibit a shear-thinning behaviour with a yield stress.

Hence, this behaviour makes them suitable candidates for various applications, as it enables them to maintain structural integrity at rest and become less viscous when subjected to shear forces, facilitating their use as binders or additives in different formulations.

Appendix B. Ageing of the alumina pastes

The ageing of both A-ALS-GG and A-ALS-P95 pastes was studied by monitoring the evolution of their viscoelastic properties over time.

Amplitude sweep tests were conducted over a period of one month. Each analysed sample was individually and tightly sealed after preparation to ensure that the measurements were not affected by paste drying. Two conditioning modes were investigated: (i) refrigeration at 4 °C or (ii) storage at room temperature (20 °C). Results are shown in Fig. B-1.

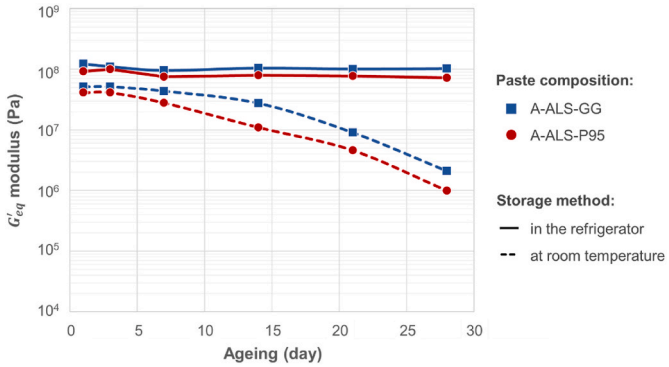

Fig. B-1. Evolution of the equivalent storage modulus in the LVER (G'_{eq}) as a function of time and the conditioning mode, for both A-ALS-GG and A-ALS-P95 pastes.

Based on dynamic measurements, the viscoelastic properties of A-ALS-GG and A-ALS-P95 pastes remain stable for one month when stored in the refrigerator. Both exhibit an equivalent storage modulus (G'_{eq}) on the order of 1.10^8 Pa and a yield stress (τ_y) ranging between 5.10^3 and 6.10^3 Pa.

In contrast, A-ALS-GG and A-ALS-P95 pastes gradually degrade when stored at room temperature. G'_{eq} progressively decreases after 7 days of ageing. In both cases, the size of the LVER reduces, indicating a loss of stability within the pastes. Their deterioration is evidenced by the progressive appearance of mold. Enzymatic activity is increasing with temperature, promoting bacterial growth. Therefore, similar to gels, refrigeration has been chosen for storing the ceramic pastes.

Printability tests were conducted concurrently with the ageing of the pastes. After one month of refrigeration, parts were successfully printed from both pastes, with a quality comparable to that obtained from freshly prepared pastes. These tests confirm the benefits of refrigeration for storage. Moreover, the usability duration of the eco-friendly formulated pastes appears promising for industrial applications.

References

[1] L. Goyos-Ball, E. García-Tuñón, E. Fernández-García, R. Díaz, A. Fernández, C. Prado, E. Saiz, R. Torrecillas, Mechanical and biological evaluation of 3D printed 10CeTZP-Al2O3 structures, J. Eur. Ceram. Soc. 37 (2017) 3151–3158, https://doi.org/10.1016/j.jeurceramsoc.2017.03.012.

[2] J.G. Dellinger, J. Cesarano III, R.D. Jamison, Robotic deposition of model hydroxyapatite scaffolds with multiple architectures and multiscale porosity for bone tissue engineering, J. Biomed. Mater. Res., Part A 82 (2007) 383–394, https://doi.org/10.1002/jbm.a.31072.

[3] G. De La Osa, D. Pérez-Coll, P. Miranzo, M.I. Osendi, M. Belmonte, Printing of Graphene Nanoplatelets into highly electrically conductive three-dimensional porous Macrostructures, Chem. Mater. 28 (2016) 6321–6328, https://doi.org/10.1021/acs.chemmater.6b02662.

[4] L. Tabard, V. Garnier, E. Prud'Homme, E.-J. Courtial, S. Meille, J. Adrien, Y. Jorand, L. Gremillard, Robocasting of highly porous ceramics scaffolds with hierarchized porosity, Addit. Manuf. 38 (2021) 101776, https://doi.org/10.1016/j.addma.2020.101776, 101776.

[5] L. Wahl, M. Weichelt, P. Goik, S. Schmiedeke, N. Travitzky, Robocasting of reaction bonded silicon carbide/silicon carbide platelet composites, Ceram. Int. 47 (2021) 9736–9744, https://doi.org/10.1016/j.ceramint.2020.12.113.

[6] J. Cesarano III, I.A. Aksay, Processing of highly concentrated aqueous α-alumina suspensions stabilized with polyelectrolytes, J. Am. Ceram. Soc. 71 (1988) 1062–1067, https://doi.org/10.1111/j.1151-2916.1988.tb05792.x.

[7] C. Duran, K. Sato, Y. Hotta, T. Nagaoka, K. Watari, Eco-friendly processing and methods for ceramic materials - a review, J. Ceram. Soc. Jpn. 116 (2008) 1175–1181, https://doi.org/10.2109/jcersj2.116.1175.

[8] M. Holler, J. Alberdi-Cedeño, A. Auñon-Lopez, T. Pointner, A. Martínez-Yusta, J. König, M. Pignitter, Polylactic acid as a promising sustainable plastic packaging for edible oils, Food Packag. Shelf Life 36 (2023) 101051, https://doi.org/10.1016/j.fpsl.2023.101051.

[9] I.S. Elizarova, L. Vandeperre, E. Saiz, Conformable green bodies: plastic forming of robocasted advanced ceramics, J. Eur. Ceram. Soc. 40 (2020) 552–557.

[10] X. Chi, Micro-extrusion of Fine Ceramic Latticework, n.d. .

[11] S. Tang, L. Yang, G. Li, X. Liu, Z. Fan, 3D printing of highly-loaded slurries via layered extrusion forming: parameters optimization and control, Addit. Manuf. 28 (2019) 546–553, https://doi.org/10.1016/j.addma.2019.05.034.

[12] C. de Melo, P.S. Garcia, M.V.E. Grossmann, F. Yamashita, L.H. Dall'Antônia, S. Mali, Properties of extruded xanthan-starch-clay nanocomposite films, Braz. Arch. Biol. Technol. 54 (2011) 1223–1333, https://doi.org/10.1590/S1516-89132011000600019.

[13] J. Bourret, I. El Younsi, M. Bienia, A. Smith, P.-M. Geffroy, J. Marie, Y. Ono, T. Chartier, V. Pateloup, Micro extrusion of innovative alumina pastes based on aqueous solvent and eco-friendly binder, J. Eur. Ceram. Soc. 38 (2018) 2802–2807, https://doi.org/10.1016/j.jeurceramsoc.2018.02.018.

[14] N. Thombare, U. Jha, S. Mishra, M.Z. Siddiqui, Guar gum as a promising starting material for diverse applications: a review, Int. J. Biol. Macromol. 88 (2016) 361–372, https://doi.org/10.1016/j.ijbiomac.2016.04.001.

[15] M. Elbadawi, M. Mosalagae, I.M. Reaney, J. Meredith, Guar gum: a novel binder for ceramic extrusion, Ceram. Int. 43 (2017) 16727–16735, https://doi.org/10.1016/j.ceramint.2017.09.066.

[16] J. Marie, J. Bourret, P.-M. Geffroy, T. Chartier, M. Bienia, V. Chaleix, L. Picton, A. Smith, Impact of bio-based binders on rheological properties of aqueous alumina slurries for tape casting, J. Eur. Ceram. Soc. (2021), https://doi.org/10.1016/j.jeurceramsoc.2021.03.049.

[17] Y. Sun, C. Peng, X. Wang, R. Wang, J. Yang, D. Zhang, Rheological behavior of Al2O3 suspensions containing polyelectrolyte complexes for direct ink writing, Powder Technol. 320 (2017) 223–229.

[18] T. Schlordt, S. Schwanke, F. Keppner, T. Fey, N. Travitzky, P. Greil, Robocasting of alumina hollow filament lattice structures, J. Eur. Ceram. Soc. 33 (2013) 3243–3248, https://doi.org/10.1016/j.jeurceramsoc.2013.06.001.

[19] S.L.; D.H.; C.J.I.I.I., D.D. King, B.H. Morissette, Influence of Rheology on Deposition Behavior of Ceramic Pastes in Direct Fabrication Systems, University of Texas at Austin, 1998.

[20] L. Wahl, M. Lorenz, J. Biggemann, N. Travitzky, Robocasting of reaction bonded silicon carbide structures, J. Eur. Ceram. Soc. 39 (2019) 4520–4526.

[21] A. Zocca, P. Colombo, C.M. Gomes, J. Günster, Additive manufacturing of ceramics: issues, Potentialities, and Opportunities, J. Am. Ceram. Soc. 98 (2015) 1983–2001, https://doi.org/10.1111/jace.13700.

[22] J.E. Smay, G. Gratson, R.F. Shepherd, J. Cesarano, J.A. Lewis, Directed colloidal assembly of 3D periodic structures, Adv. Mater. 14 (2002) 1279–1283, https://doi.org/10.1002/1521-4095(20020916)14:18<1279::AID-ADMA1279>3.0.CO;2-A.

[23] A. M'Barki, L. Bocquet, A. Stevenson, Linking rheology and printability for dense and strong ceramics by direct ink writing, Sci. Rep. 7 (2017) 6017, https://doi.org/10.1038/s41598-017-06115-0.

[24] S.S.L. Chan, M.L. Sesso, G.V. Franks, Direct ink writing of hierarchical porous alumina-stabilized emulsions: rheology and printability, J. Am. Ceram. Soc. 103 (2020) 5554–5566, https://doi.org/10.1111/jace.17305.

[25] W.J. Costakis, L.M. Rueschhoff, A.I. Diaz-Cano, J.P. Youngblood, R.W. Trice, Additive manufacturing of boron carbide via continuous filament direct ink writing of aqueous ceramic suspensions, J. Eur. Ceram. Soc. 36 (2016) 3249–3256, https://doi.org/10.1016/j.jeurceramsoc.2016.06.002.

[26] A. Corker, H.C.-H. Ng, R.J. Poole, E. García-Tuñón, 3D printing with 2D colloids: designing rheology protocols to predict 'printability' of soft-materials, Soft Matter 15 (2019) 1444–1456, https://doi.org/10.1039/C8SM01936C.

[27] M. Maillard, J. Chevalier, L. Gremillard, G.P. Baeza, E.-J. Courtial, S. Marion, V. Garnier, Optimization of mechanical properties of robocast alumina parts through control of the paste rheology, 17th Eur. Inter-Reg. Conf. Ceram. 43 (2023) 2805–2817, https://doi.org/10.1016/j.jeurceramsoc.2022.12.008.

[28] S. Lamnini, H. Elsayed, Y. Lakhdar, F. Baino, F. Smeacetto, E. Bernardo, Robocasting of advanced ceramics: ink optimization and protocol to predict the printing parameters - a review, Heliyon 8 (2022) e10651, https://doi.org/10.1016/j.heliyon.2022.e10651.

[29] H. Liu, Y. Li, D. Li, Research on rheological properties and extrusion behavior of aqueous alumina paste in paste-extrusion-based SFF processes, Int. J. Adv. Manuf. Technol. 83 (2016) 2039–2047, https://doi.org/10.1007/s00170-015-7720-z.

[30] P.-F. Mougard Camacho, F. Doreau, A. Poulesquen, R. Castellani, R. Valette, Extrusion as a novel production method for MOX (UO2-PuO2) fuel rods: rheological and physical characterizations on surrogate pastes, J. Eur. Ceram. Soc. (2021), https://doi.org/10.1016/j.jeurceramsoc.2021.01.031.
[31] D. Stewart, Lignin as a base material for materials applications: chemistry, application and economics, Ind. Crops Prod. 27 (2008) 202–207, https://doi.org/10.1016/j.indcrop.2007.07.008.
[32] C.G. Yoo, A.J. Ragauskas, Opportunities and challenges of lignin utilization, in: C. G. Yoo, A. Ragauskas (Eds.), ACS Symp. Ser., American Chemical Society, Washington, DC, 2021, pp. 1–12, https://doi.org/10.1021/bk-2021-1377.ch001.
[33] J. Marie, J. Bourret, P.-M. Geffroy, A. Smith, V. Chaleix, T. Chartier, Eco-friendly alumina suspensions for tape-casting process, J. Eur. Ceram. Soc. 37 (2017) 5239–5248, https://doi.org/10.1016/j.jeurceramsoc.2017.04.033.
[34] M.G. Papich, Psyllium, in: Papich Handb. Vet. Drugs, Elsevier, 2021, pp. 795–796, https://doi.org/10.1016/B978-0-323-70957-6.00462-3.
[35] A. Farahnaky, H. Askari, M. Majzoobi, Gh Mesbahi, The impact of concentration, temperature and pH on dynamic rheology of psyllium gels, J. Food Eng. 100 (2010) 294–301, https://doi.org/10.1016/j.jfoodeng.2010.04.012.
[36] R. Lapasin, S. Pricl, Rheology of Industrial Polysaccharides: Theory and Applications, first ed., Springer US, 1995 https://doi.org/10.1007/978-1-4615-2185-3. (Accessed 25 March 2020).
[37] D. Gourdonnaud, V. Pateloup, A. Junger, J. Bourret, T. Chartier, P.-M. Geffroy, Correlation between filament deposition path, microstructural and mechanical properties of dense alumina parts printed by robocasting, J. Eur. Ceram. Soc. (2023), https://doi.org/10.1016/j.jeurceramsoc.2023.09.067.
[38] A. Entezari, N.C. Liu, I. Roohani, Z. Zhang, J. Chen, B. Sarrafpour, H. Zoellner, M. Behi, H. Zreiqat, Q. Li, On design for additive manufacturing (DAM) parameter and its effects on biomechanical properties of 3D printed ceramic scaffolds, Mater. Today Commun. 23 (2020) 101065, https://doi.org/10.1016/j.mtcomm.2020.101065.
[39] L. Palmqvist, K. Holmberg, Dispersant adsorption and viscoelasticity of alumina suspensions measured by quartz crystal microbalance with dissipation monitoring and in Situ dynamic rheology, Langmuir 24 (2008) 9989–9996, https://doi.org/10.1021/la800719u.
[40] L. Picton, D. Le Cerf, Chromatographie D'exclusion Stérique Multi-Détection, Actual, Chim., 2017, pp. 59–64.
[41] M.M. Bradford, A rapid and sensitive method for the quantitation of microgram quantities of protein utilizing the principle of protein-dye binding, Anal. Biochem. 72 (1976) 248–254, https://doi.org/10.1016/0003-2697(76)90527-3.
[42] D. Gourdonnaud, Micro-extrusion de pâtes céramiques innovantes respectueuses de l'environnement : relation entre formulation, imprimabilité, stratégie de dépôt et propriétés mécaniques des pièces frittées, University of Limoges, 2022. PhD thesis, https://www.theses.fr/2022LIMO0135. (Accessed 8 February 2023).
[43] E.B. Bagley, End corrections in the capillary flow of polyethylene, J. Appl. Phys. 28 (1957) 624–627, https://doi.org/10.1063/1.1722814.
[44] B. Rabinowitsch, Über die Viskosität und Elastizität von Solen, Z. Für Phys. Chem. 145A (1929) 1–26, https://doi.org/10.1515/zpch-1929-14502.
[45] W.H. Herschel, R. Bulkley, Konsistenzmessungen von Gummi-Benzollösungen, Kolloid Z. 39 (1926) 291–300, https://doi.org/10.1007/BF01432034.
[46] D18 Committee, ASTM D4318-17e1 - Test Methods for Liquid Limit, Plastic Limit, and Plasticity Index of Soils, ASTM Int., n.d. https://doi.org/10.1520/D4318-17E01. .
[47] A. Temyingyong, K. Chantawarangul, P. Sudasna-na-Ayudthya, Statistical analysis of influenced factors affecting the plastic limit of soils, Kasetsart J./Nat. Sci. 36 (2002) 98–102.
[48] M. Kornmann, Complementary explanation of the Bigot' curve, Ind. Ceram. Verriere (2006) 44–53.
[49] S. Oummadi, B. Nait-Ali, A. Alzina, M.-C. Paya, J.-M. Gaillard, D.S. Smith, Optical method for evaluation of shrinkage in two dimensions during drying of ceramic green bodies, Open Ceram. 2 (2020) 100016, https://doi.org/10.1016/j.oceram.2020.100016.
[50] A. Bigot, Retrait au séchage des kaolins et argiles, 1921. Paris.
[51] G.W. Scherer, Theory of drying, J. Am. Ceram. Soc. 73 (1990) 3–14, https://doi.org/10.1111/j.1151-2916.1990.tb05082.x.
[52] ASTM International, ASTM B962-17 - Test Methods for Density of Compacted or Sintered Powder Metallurgy (PM) Products Using Archimedes Principle, ASTM International, 2017, https://doi.org/10.1520/B0962-17.
[53] E. Feilden, Additive Manufacturing of Ceramics and Ceramic Composites via Robocasting, Thèse de doctorat, Unpublished, 2017, https://doi.org/10.13140/RG.2.2.29343.25765. (Accessed 7 April 2022).
[54] J. Baltazar, P.M.C. Torres, J. Dias-de-Oliveira, J. Pinho-da-Cruz, S. Gouveia, S. Olhero, Influence of filament patterning in structural properties of dense alumina ceramics printed by robocasting, J. Manuf. Process. 68 (2021) 569–582, https://doi.org/10.1016/j.jmapro.2021.05.043.
[55] D. Gourdonnaud, V. Pateloup, A. Junger, J. Bourret, T. Chartier, P.-M. Geffroy, Correlation between filament deposition path, microstructural and mechanical properties of dense alumina parts printed by robocasting, J. Eur. Ceram. Soc. 44 (2024) 1027–1035, https://doi.org/10.1016/j.jeurceramsoc.2023.09.067.
[56] K. te Nijenhuis, Thermoreversible Networks: Viscoelastic Properties and Structure of Gels, Springer, 1997.